JOURNAL OF PETROLOGY | VOLUME 43 | NUMBER 1 | PAGES 85–101 | 2002

Crystal Size Distributions and Scaling Laws in the Quantification of Igneous Textures

M. J. ZIEG AND B. D. MARSH*

MORTON K. BLAUSTEIN DEPARTMENT OF EARTH AND PLANETARY SCIENCE, JOHNS HOPKINS UNIVERSITY, BALTIMORE, MD 21218, USA

RECEIVED JANUARY 15, 2001; REVISED TYPESCRIPT ACCEPTED JULY 11, 2001

This study demonstrates the value of the combined use of scaling analysis and crystal size distribution (CSD) measurements in the interpretation of igneous textures and outlines applications of these methods to other fundamentally important problems. Theoretical calculations and measurements of natural samples are used to characterize the relationship between igneous texture and cooling history. The total number (N_T) and mean length ($\bar{L}$) of crystals in a sample are correlated through a scaling relationship of the form $N_T^{-1/3} \propto \bar{L}$. This proportionality depends on the mineralogy of the rock, and so a modal normalization factor (C) is introduced. The CSD slope, S, and intercept, ln(n°), are uniquely related to each other through the equation ln(n°) = 4ln(S) − ln(C), where $S = \bar{L}^{-1}$. This overall relationship allows the texture of a rock to be related to the local duration of cooling through an arbitrary crystal growth model. Quantification of the link between the texture of a rock and its cooling history makes it possible to predict spatial variations in texture. We show an example of this method using the Sudbury Igneous Complex, Canada. Additional applications include relating the textures of volcanic rocks to spatial and temporal variations in the magma chamber and extracting kinetic parameters from suites of comagmatic rocks.

KEY WORDS: *crystal size distributions; crystallization kinetics; magmatic processes; texture*

INTRODUCTION

The textures of igneous rocks record the physical history of crystallization. As magma cools, crystals nucleate and grow. Because these minerals have different compositions than the magma, the chemistry of the liquid changes as it cools and precipitates new minerals. Systematic studies of the chemical evolution of cooling magmas have investigated the detailed relationships between temperature, phase abundance, and phase composition. The reaction series (Bowen, 1922) and the CIPW norm (Cross *et al.*, 1903) have been supplemented by modern thermodynamic models that predict the compositions and abundances of minerals in equilibrium with melt of a given composition and temperature (e.g. Ariskin *et al.*, 1993; Ghiorso & Sack, 1995). Although there are a few areas of uncertainty, the chemistry of igneous petrogenesis is fairly well understood.

But chemical models cannot address the central problem of igneous crystallization, which is the physical process of generating a set of crystals from magma. Two magmas with the same composition will normally produce the same minerals in the same proportions. However, depending on their thermal histories, these two magmas can solidify into rocks with drastically different physical appearances (e.g. basalt and gabbro). The set of minerals is the same, but what distinguishes them is the abundance and size of the constituent crystals.

The fine-grained rocks in the chilled margins of most basic intrusions cooled rapidly and the coarse-grained rocks in the interiors of plutons cooled slowly. This has been clear for many years, and many methods have been proposed to quantify the relationship between grain size and position within mafic sills and dikes (Lane, 1899, 1903, 1928; Queneau, 1902; Winkler, 1949; Gray, 1970, 1978). These studies have pointed out the potential value of textural analysis as a tool in igneous petrology. Cashman (1993) has compiled the results of numerous earlier works on plagioclase crystallization and presented correlations between the crystallization kinetics and cooling rate. In this study, the focus is on developing quantitative relationships between the ultimate texture

*Corresponding author. Telephone: (410) 516-7034. Fax: (410) 516-7933. E-mail: bmarsh@jhu.edu

of a rock and its cooling history. On the basis of these relationships, crystal size distributions (CSDs) can be directly connected to modal mineralogy and solidification history without relying on precise kinetic models. We establish a general method for estimating the distribution of crystal sizes as a function of position in any intrusive igneous body. The method is direct, and can be included easily in crystallization computations.

To begin, we will describe the dataset used in this study. Analytical results from scaling theory will then be used to reveal a basic relationship between the abundance and mean size of crystals in a rock. Using measured textures, this relationship will be examined and calibrated; the result is a fundamental link between CSD intercept and slope. Finally, the intercept–slope relationship will be used together with the original scaling equations to compute CSD variation as a function of the local cooling history in crystallizing bodies.

DATA

Although this work is primarily based on theoretical considerations, it is critical to verify these predictions using information from real rocks. To ensure accuracy, we have manually traced and measured an average of 1000 plagioclase crystals in each of 60 samples of norite and diabase from the Sudbury Igneous Complex and the Ferrar Dolerite. These samples were specifically chosen to cover a range of mineralogies and cooling histories. Because these rocks are all intrusive, we will also make comparisons with published textural measurements from volcanic rocks.

The Sudbury Igneous Complex (SIC), located in Ontario, Canada (Fig. 1) was formed at 1850 Ma as an impact melt sheet (Dietz, 1964; Grieve, 1994). It is $\sim 2{\cdot}5$ km thick, with the upper two-thirds consisting of granophyre and the bottom third consisting of norite. The norite consists of 50% plagioclase and 25% orthopyroxene with abundant ($\sim 25\%$) interstitial quartz and granophyric intergrowth; it is locally referred to as felsic norite. At the base of the norite, the orthopyroxene abundance increases to 50% and plagioclase decreases to 25%; this phase is referred to as mafic norite. Excellent reviews of the petrography and petrology of the SIC have been presented by, among others, Naldrett *et al.* (1970) and Pye *et al.* (1984).

The Ferrar Dolerites are Jurassic rift-related tholeiites that occur throughout the Trans-Antarctic Mountains, and are particularly voluminous in the McMurdo Dry Valleys (Gunn, 1966). The samples used in this study are from the Basement and Peneplain sills of the Dry Valleys (Fig. 2). The Peneplain Sill is uniform diabase, containing approximately 35% calcic pyroxene and 45% plagioclase. The Basement Sill has margins composed of uniform diabase (45% clinopyroxene, 45% plagioclase) and an extensive central zone of coarse orthopyroxene–plagioclase cumulate (60% orthopyroxene, 35% plagioclase). The nature and origin of this cumulate zone have been discussed by Marsh & Philipp (1996) and Marsh (2000).

Crystal size distributions (CSDs) were obtained for each of the samples by manually tracing all of the plagioclase crystals on a digital image of a thin section, then measuring the long axis of each. Stereological corrections were performed and a CSD was calculated using the computer program CSDCorrections 1.1 (Higgins, 2000). The CSDs are generally simple, as shown in Fig. 3, and can be described very well by means of a straight line. The slope and intercept of each fitted line are given in Table 1, along with calculated uncertainties. Also listed are the average crystal length and total number of crystals, as measured directly from the thin section, the maximum observed crystal length, and the modal plagioclase fraction.

SCALING ANALYSIS OF BASIC RELATIONS

Equations

Because of the inherent analytical and physical complexity of crystallization kinetics (e.g. Swanson, 1977; Dowty, 1980; Kirkpatrick, 1983), it is convenient to have a set of equations that are simple, but still preserve the first-order attributes of the complete system. Scaling is especially useful when the exact values or functional relationships of several parameters are unknown. In a scaling analysis, only the dimensions and relative magnitudes of the parameters that characterize a process are used to evaluate the form of the controlling relationships.

A set of scaling equations (Marsh, 1998; see also Brandeis & Jaupart, 1987*b*) relates the characteristic number of crystals [N_0 (cm^{-3})], crystal size [L_0 (cm)], and crystallization time [t_c (s)] in a rock to the characteristic rates of nucleation and growth [$\mathcal{J}_0$ (cm^{-3}/s) and G_0 (cm/s)]:

$$N_0 = C_N \left(\frac{\mathcal{J}_0}{G_0} \right)^{3/4} \tag{1}$$

$$L_0 = C_L \left(\frac{G_0}{\mathcal{J}_0} \right)^{1/4} \tag{2}$$

$$t_c = C_t (G_0^3 \mathcal{J}_0)^{-1/4} \tag{3}$$

where C_N, C_L, and C_t are dimensionless constants. These relationships do not depend on the ultimate functional forms describing the nucleation and growth rates, only the characteristic magnitudes of these functions. In other

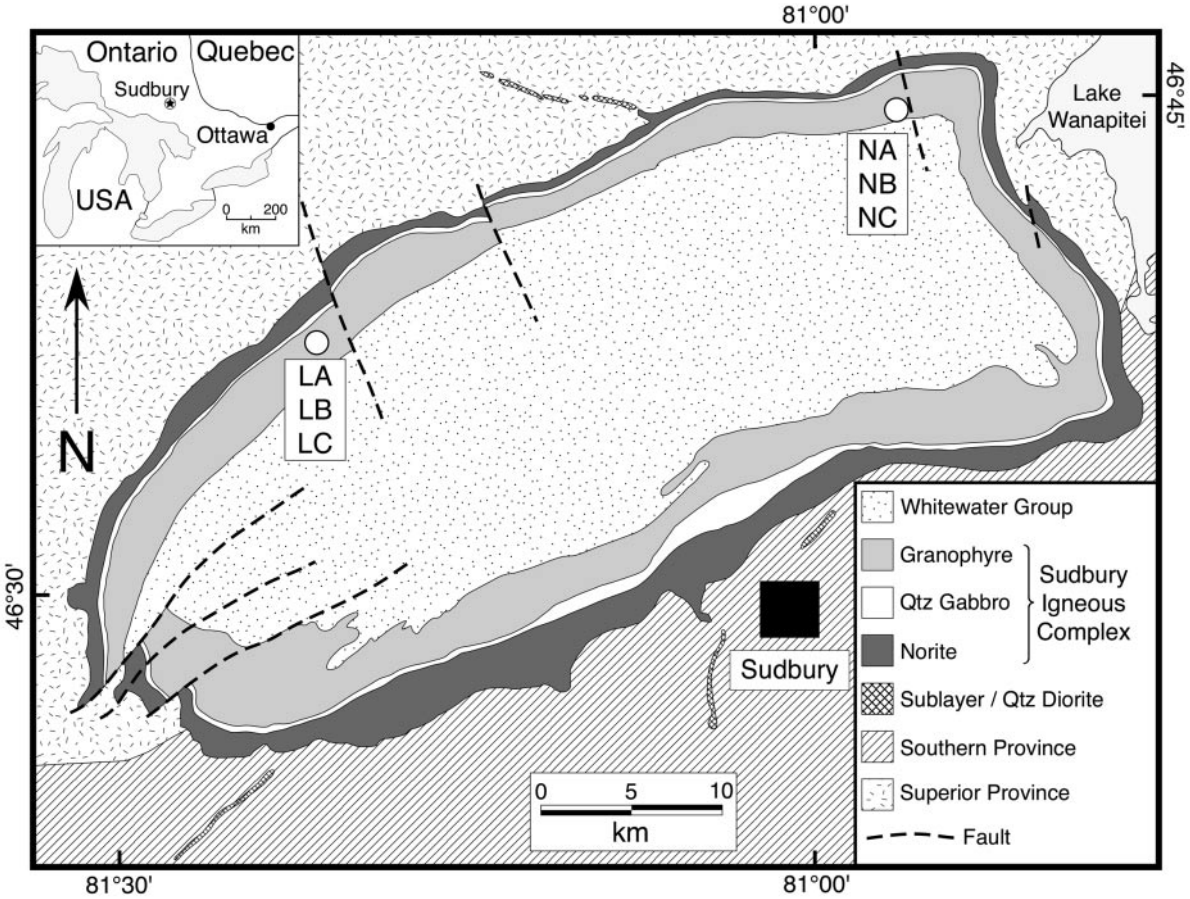

Fig. 1. General geology of Sudbury Igneous Complex, Ontario, with drill core locations. Adapted from Naldrett & Kullerud (1967) and Dressler *et al.* (1996).

words, these equations hold whether the growth rate is constant, size dependent, temperature dependent, or depends on other parameters. The drawback of such relations is that the details of the temporal evolution of N and L cannot be found. This is analogous to knowing the amplitude of a wave, but not its form.

Direct use of these equations requires values for the characteristic rates of nucleation and growth, which are generally not well known (but see Marsh, 1998). However, by combining equations (1) and (2) into a single relationship between L_0 and N_0, the direct dependence on growth and nucleation rates can be eliminated, yielding

$$L_0 = (CN_0)^{-1/3} \tag{4}$$

where C_L and C_N have been combined into a single constant C. Equation (4) provides a quantitative link between the characteristic crystal size in a rock (L_0) and the characteristic number of crystals in the rock (N_0). Here the role of dimensional homogeneity in scaling is clear: to match the dimensions of L_0 (cm), N_0 (cm^{-3}) must be raised to the $-1/3$ power. This equation is not new (e.g. Cashman, 1993), and although its fundamental importance is not immediately obvious, it will be made clear below.

Equations (1) and (2) can also be combined with (3) to determine the dependence of L_0 and N_0 on t_c and G_0:

$$L_0 = \frac{C_L}{C_t} G_0 t_c \tag{5}$$

$$N_0 = C_N C_t^3 (G_0 t_c)^{-3}. \tag{6}$$

Equation (5) predicts that L_0 varies linearly with t_c. This means that the rate of change of the characteristic crystal size is a constant, even though the actual growth rate for any individual crystal is likely to be a more complex function of time, temperature, and other variables. Equation (6) shows the complex interrelationship that actually exists between the different parameters. For a fixed characteristic time (t_c), a slow effective growth rate (G_0) results in a greater number of crystals. For a fixed value of G_0, a greater value of t_c will result in a smaller number of crystals. Equations (5) and (6) therefore

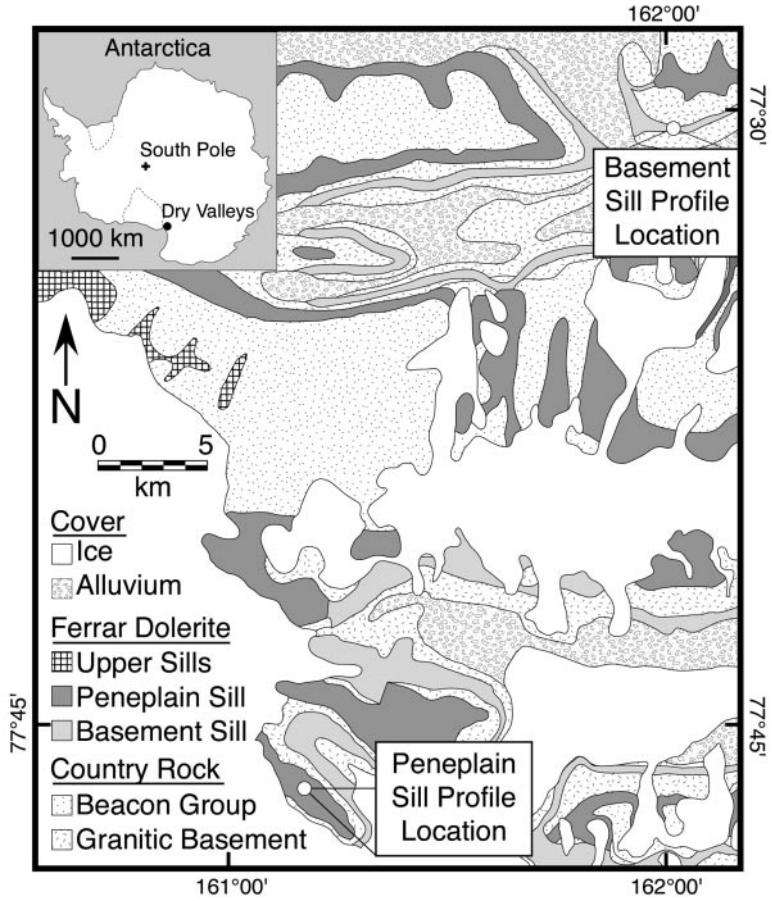

Fig. 2. General geology of Ferrar Dolerites, Dry Valleys, Antarctica, with sampling profile locations.

correspond to the qualitative observation that quickly cooled rocks (small t_c) are fine grained (small L_0, large N_0) and that slowly cooled rocks (large t_c) are coarse grained (large L_0, small N_0).

To quantify relationship (4) between N_0 and L_0 (by finding C), it is necessary to define a characteristic number and length that can be accurately and easily measured in samples. The mean length of the crystals in a sample ($\bar{L}$) was chosen as the characteristic length of crystals in the system, and the total number of crystals per unit volume (N_T) was chosen as the characteristic number of crystals. The choice of N_T as the characteristic number is obvious, but the choice of $\bar{L}$ is not. The maximum crystal length (L_{max}) would seem preferable for several reasons. First, it allows the definition of nondimensional numbers (N/N_0) and lengths (L/L_0) that vary between zero and one. By scaling on $\bar{L}$, the nondimensional length has no clear upper limit. Second, L_{max} is directly related to N_T, which can be defined as the number of crystals, per unit volume, with a length between zero and L_{max}. Finally, the maximum crystal size can also be related to the characteristic time for the system, t_c. If t_c is defined as the time required for the magma to cool from the liquidus to the solidus, L_{max} is the length of a crystal that has been growing for the entire time t_c. Any smaller crystals have grown for a shorter time interval.

The main difficulty with using the maximum crystal length rather than the mean length is that L_{max} is impractical to measure. There are fewer large crystals in a sample than small, and it is impossible to be certain that the largest crystal measured is the largest in the rock. The mean length is substituted for the maximum length because although $\bar{L}$ has less physical significance than L_{max}, it is also less dependent on the intersection and measurement of specific crystals. It is a more stable and precise measurement.

CSD calculations

As discussed above, a rock sample can be characterized by the mean length of the crystals and the total number of crystals per unit volume. These values can be obtained directly from a crystal size distribution (Marsh, 1988,

Table 1: Measured CSDs and other textural parameters

Sample	S (σ_{slope}) (cm^{-1})	$\ln(n^{\circ})$ (σ_{int}) (cm^{-4})	$\bar{L}_{Area}$ (cm)	N_{Area} (cm^{-2})	L_{max} (cm)	X_{plg}
Sudbury						
LA-115	18·02 (0·75)	10·28 (0·11)	0·1195	86·13	0·491	0·516
LA-129	21·62 (0·83)	11·03 (0·11)	0·1003	121·03	0·465	0·528
LA-135	22·93 (0·79)	11·17 (0·10)	0·0948	130·24	0·505	0·584
LA-140	26·10 (1·18)	11·67 (0·12)	0·0790	174·30	0·361	0·483
LA-145	27·69 (0·75)	11·82 (0·07)	0·0741	177·59	0·439	0·522
LA-146	28·47 (0·80)	11·99 (0·08)	0·0720	204·26	0·397	0·544
LA-148	28·12 (0·73)	11·91 (0·07)	0·0749	185·65	0·478	0·524
LA-149	28·49 (0·70)	12·11 (0·06)	0·0690	229·13	0·480	0·529
LA-155	34·24 (1·34)	12·64 (0·11)	0·0604	264·99	0·349	0·479
LA-161	35·35 (0·86)	12·85 (0·07)	0·0590	299·69	0·350	0·513
LA-164	33·37 (1·00)	12·55 (0·08)	0·0606	261·41	0·330	0·465
LB-80	19·52 (1·02)	10·50 (0·14)	0·1119	87·65	0·554	0·473
LB-91	20·67 (0·87)	10·69 (0·12)	0·1072	93·70	0·464	0·526
LB-100	22·39 (1·15)	10·97 (0·14)	0·0992	104·82	0·387	0·509
LB-110	23·69 (0·95)	11·17 (0·12)	0·0947	116·97	0·458	0·469
LB-120	26·89 (1·29)	11·93 (0·13)	0·0737	212·42	0·378	0·567
LB-130	39·27 (1·37)	13·16 (0·10)	0·0542	321·18	0·275	0·460
LB-135	42·23 (1·51)	13·50 (0·10)	0·0472	422·08	0·239	0·490
LC-91	23·27 (0·75)	11·21 (0·09)	0·0914	128·72	0·587	0·534
LC-98	21·30 (0·70)	10·90 (0·09)	0·0948	122·49	0·556	0·518
LC-110	24·39 (0·76)	11·46 (0·09)	0·0849	162·54	0·507	0·536
LC-117	28·75 (0·82)	12·00 (0·08)	0·0701	203·50	0·394	0·540
LC-124	34·69 (0·94)	12·77 (0·08)	0·0623	278·81	0·281	0·530
LC-128	33·86 (0·89)	12·63 (0·07)	0·0598	273·71	0·293	0·504
LC-129	31·38 (0·89)	12·48 (0·08)	0·0622	269·83	0·402	0·554
LC-131	33·39 (0·56)	12·60 (0·05)	0·0599	268·77	0·254	0·481
LC-133	34·47 (0·89)	12·60 (0·07)	0·0592	255·46	0·324	0·487
LC-137	34·89 (0·94)	12·71 (0·07)	0·0575	279·83	0·301	0·495
LC-139	46·33 (1·56)	13·84 (0·09)	0·0477	469·14	0·237	0·503
NA-55	30·80 (1·58)	12·15 (0·14)	0·0705	179·29	0·284	0·418
NA-64	21·12 (1·17)	10·60 (0·16)	0·1117	82·66	0·611	0·450
NA-72	26·80 (0·92)	11·58 (0·09)	0·0754	152·28	0·434	0·454
NA-79	35·32 (0·85)	12·73 (0·07)	0·0589	277·75	0·369	0·455
NB-40	20·78 (0·86)	10·65 (0·11)	0·1046	93·76	0·443	0·433
NB-49	20·85 (0·87)	10·68 (0·12)	0·1053	94·09	0·517	0·393
NB-51	31·31 (0·88)	12·14 (0·08)	0·0655	191·00	0·413	0·453
NB-54	31·24 (0·82)	12·20 (0·07)	0·0655	206·42	0·392	0·426
NB-55	28·79 (0·92)	11·80 (0·09)	0·0744	157·42	0·353	0·453
NB-56	31·11 (0·99)	12·33 (0·09)	0·0645	236·80	0·400	0·488
NB-57	35·49 (1·23)	12·79 (0·09)	0·0550	300·50	0·302	0·505
NB-60	39·99 (1·42)	13·26 (0·10)	0·0522	356·60	0·260	0·429
NC-68	17·75 (1·02)	9·99 (0·16)	0·1230	59·55	0·473	0·418
NC-75	20·29 (0·87)	10·63 (0·13)	0·1020	98·45	0·428	0·477
NC-82	24·06 (1·15)	11·28 (0·09)	0·0848	133·42	0·495	0·439
NC-86	28·90 (0·95)	11·93 (0·07)	0·0700	182·13	0·398	0·458
NC-92	32·87 (1·29)	12·47 (0·07)	0·0629	243·48	0·416	0·453

Table 1: continued

Sample	S (σ_{slope}) (cm^{-1})	$\ln(n^\circ)$ (σ_{int}) (cm^{-4})	$\bar{L}_{Area}$ (cm)	N_{Area} (cm^{-2})	L_{max} (cm)	X_{plg}
Peneplain Sill						
PPS-270	70·96 (2·37)	15·34 (0·09)	0·0306	847·11	0·132	0·406
PPS-271	74·84 (2·25)	15·42 (0·08)	0·0272	911·30	0·133	0·332
PPS-273	90·48 (2·69)	16·23 (0·08)	0·0221	1462·75	0·119	0·385
PPS-275	101·46 (2·88)	16·70 (0·08)	0·0204	1748·56	0·136	0·366
PPS-276	88·72 (2·74)	16·27 (0·08)	0·0230	1527·40	0·105	0·388
96-PPS-1	83·36 (2·78)	15·94 (0·09)	0·0249	1190·22	0·124	0·322
96-PPS-5	93·88 (2·11)	16·54 (0·06)	0·0224	1687·33	0·109	0·379
Basement Sill						
A-36	224·91 (7·24)	19·67 (0·09)	0·0101	6216·84	0·055	0·341
A-37	393·46 (14·53)	22·02 (0·10)	0·0059	19536·68	0·023	0·272
A-100A	389·63 (14·31)	22·01 (0·11)	0·0069	15996·78	0·029	0·315
A-100B	199·59 (6·55)	19·46 (0·09)	0·0112	6297·09	0·048	0·365
A-104	213·56 (6·89)	19·35 (0·09)	0·0104	5223·19	0·050	0·263
A-105	389·88 (13·58)	21·84 (0·11)	0·0067	15000·00	0·048	0·313
A-106	481·41 (19·31)	22·69 (0·12)	0·0046	27018·18	0·019	0·215

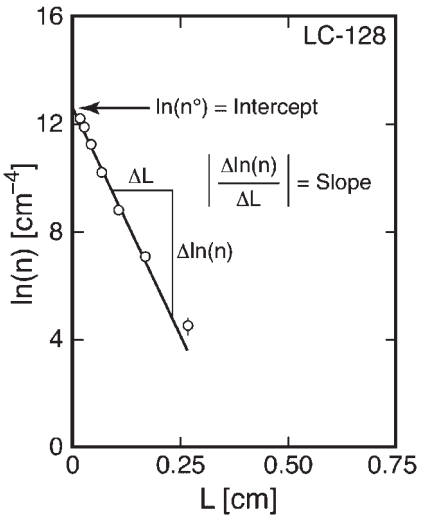

Fig. 3. Example CSD. The slope and intercept are obtained from a best-fit approximation to the measured data points. Although CSD slopes are always negative, we refer to them as positive numbers.

1998). CSDs of many crystallizing systems in both industry and nature can be approximated as straight lines described by an equation of the form

$$\ln[n(L)] = \ln(n^\circ) - SL. \quad (7)$$

The population density $n(L)$ is defined as the number of crystals per volume per length, as a function of crystal size L; $\ln(n^\circ)$ and S are the intercept and absolute value of the slope, respectively, of a linear approximation to the CSD (see Fig. 3). The population density can also be obtained explicitly by rewriting equation (7):

$$n(L) = n^\circ \exp(-SL). \quad (8)$$

The cumulative distribution $\mathcal{N}(L)$, the number of crystals smaller than L, can be obtained from the CSD by integrating the population density over the size range from zero to L:

$$\mathcal{N}(L) \equiv \int_0^L n(L)\,dL = \frac{n^\circ}{S}[1 - \exp(-SL)]. \quad (9)$$

The total number of crystals, $\mathcal{N}_T$, is found by integrating the population density over the entire size range from zero to infinity (or zero to L_{max}, if known):

$$\mathcal{N}_T \equiv \int_0^\infty n(L)\,dL = \frac{n^\circ}{S}. \quad (10)$$

The upper limit of integration is not given in terms of L_{max} for two reasons. As mentioned above, the true maximum crystal length is generally difficult to determine accurately. More importantly, the population density at high values of L is generally very low (note that a CSD diagram shows the natural logarithm of the population density), and the number density of crystals projected beyond L_{max} is very small relative to the number of crystals between zero and L_{max}. Thus, the contribution

made to $\mathcal{N}_T$ in equation (10) by continuing the integral in the size interval from L_{max} to infinity is negligible.

The total length (L_T) of all the crystals in a sample can be obtained from the first moment of the population density equation [see Marsh (1988) and Randolph & Larson (1988) for details]. That is,

$$L_T \equiv \int_0^\infty Ln(L)\,dL = \frac{n^\circ}{S^2}. \quad (11)$$

The mean length can then be calculated from equations (10) and (11):

$$\bar{L} \equiv \frac{L_T}{\mathcal{N}_T} = \frac{1}{S}. \quad (12)$$

Equations (10) and (12) define the characteristic number and characteristic length scales of the sample in terms of the population density equation (8). These two variables are fully consistent with each other, are easily measured, and can be used to test and calibrate equation (4). In the following sections, they will be referred to frequently.

Calibration of number–length relationship

The significance of equations (10) and (12) is that they provide a link between generic scaling relationships and quantitative textural measurements. That is, equation (4) can be rewritten as

$$\mathcal{N}_T^{-1/3} = C^{1/3}\,\bar{L}. \quad (13)$$

This result predicts a linear relationship between the inverse cube root of $\mathcal{N}_T$ and $\bar{L}$. Figure 4a shows a plot of these values, calculated from data in Table 1. In this plot, there is a reasonably clear linear relationship. However, careful inspection shows that the data follow two similar, but distinct trends.

For a given value of $\bar{L}$, the Ferrar Dolerite samples have a slightly lower total number (higher $\mathcal{N}_T^{-1/3}$) than the SIC felsic norite samples. This difference is due to the different modal mineralogies of the two suites (see Table 1). Although the size of any given crystal depends only on its growth history, the total number of crystals of a particular phase is strongly influenced by the bulk mineralogy of the rock. For example, let us consider a high-alumina basalt (HAB) and a picrite. The HAB contains significantly more modal plagioclase than the picrite. However, if these two magmas follow identical cooling paths, the plagioclase crystals in both rocks will have similar sizes. The much lower modal plagioclase content of the picrite will be reflected in fewer, not smaller, plagioclase crystals. This effect can be shown explicitly by rewriting equation (13):

$$\mathcal{N}_T\bar{L}^3 = C^{-1}. \quad (14)$$

When $\mathcal{N}_T\bar{L}^3$ is compared with the observed modal abundance of plagioclase X_{plg} (Fig. 4b), there is a clear correlation:

$$\mathcal{N}_T\bar{L}^3 = 0{\cdot}48X_{plg} = C^{-1} \quad (15)$$

which is simply a restatement of the conservation of mass condition. The number of crystals per unit volume ($\mathcal{N}_T$) times a characteristic crystal volume ($\bar{L}^3$) must be directly related to the volumetric proportion of that mineral in the rock.

As $\mathcal{N}_T$ is more sensitive than $\bar{L}$ to the abundance of plagioclase in the system, it can be adjusted to eliminate the effect of varying mode. That is, a normalized total number ($\mathcal{N}_N$) can be defined using equation (15):

$$\mathcal{N}_N \equiv C\mathcal{N}_T = 2{\cdot}08\mathcal{N}_T\,X_{plg}^{-1}. \quad (16)$$

A similar modal correction factor ($C = X^{-1}$) was proposed by Higgins (1999). It should be noted that in this method, the value of C (i.e. $2{\cdot}08\ X_{plg}^{-1}$) will depend on the mineral being studied and, to a much lesser extent, on the detailed method of measurement and data reduction used to calculate the CSD. We have experimented with two methods of CSD calculation, and found only very minor differences in the results.

The results of this normalization are shown in Fig. 4c. The correlation is significantly improved. Low-plagioclase Ferrar Dolerites are now in agreement with the trend defined by the high-plagioclase SIC norites.

CSD intercept–slope correlation

It should be emphasized that the relationship between mean crystal length and total number [equation (13)], although ultimately based in kinetic theory, is not in itself a central conclusion. Rather, it is a valuable quantitative relationship for reducing the number of variables in the system, especially in intrusive rocks. Rather than considering the numbers and sizes separately, Fig. 4 shows that it is sufficient to measure only one, and because of the conservation of mass condition in equation (15), the other can be calculated accurately. In this section, it will be shown that this one relationship allows the entire spectrum of crystal sizes to be predicted accurately from a knowledge of only one of these parameters ($\bar{L}$ or $\mathcal{N}_T$).

In equations (10) and (12), $\mathcal{N}_T$ and $\bar{L}$ are quantitatively related to the CSD intercept and slope. Equation (10) can be rearranged as

$$n^\circ = \mathcal{N}_T S. \quad (17)$$

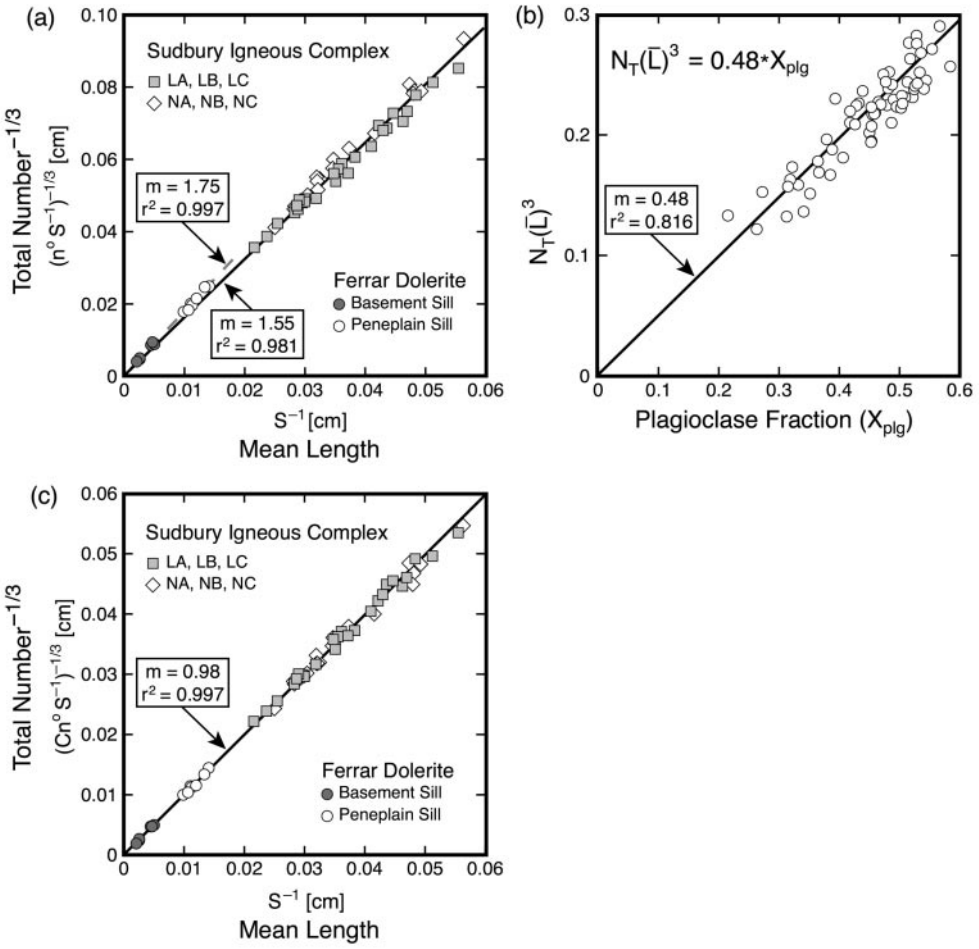

Fig. 4. (a) Relationship between $\mathcal{N}_T^{-1/3}$ and $\bar{L}$. Total number and mean length are calculated from CSD slopes and intercepts (Table 1). The Antarctic samples follow a slightly higher trend than the Sudbury samples. This indicates that for the same mean length, there will be a smaller total number of crystals (per cm^3) in a sample of Antarctic diabase than in a sample of felsic norite from the SIC. (b) The effect of modal plagioclase. If mean grain size is assumed to be independent of modal mineralogy in a rock, then the total number of crystals in a rock will be proportional to the plagioclase abundance. (c) Relationship between $\mathcal{N}_T^{-1/3}$ and $\bar{L}$. The total number is corrected for the effect of varying modal plagioclase content in the rocks.

Using equation (13) to eliminate $\mathcal{N}_T$, and substituting equation (12), this reduces to

$$n^\circ = C^{-1}\bar{L}^{-3}S = C^{-1}S^4 \tag{18}$$

or

$$\ln(n^\circ) = 4\ln(S) - \ln(C). \tag{19}$$

This completely general relationship between intercept and slope is demonstrated, for both the high-plagioclase, coarse-grained Sudbury norites and the low-plagioclase, fine-grained Antarctic dolerites, in Fig. 5. The basic form is set by the first term on the right-hand side in equation (19). The modal variations and the exact means of data reduction used in obtaining the CSD are taken into account in the second term. Because the relationship between C and X_{plg} has been calibrated [equation (15)], the different curves can be related directly to different modal plagioclase contents.

The same relationship between CSD intercept and slope is shown in Fig. 6 for published CSD data (Cashman, 1992; Crisp *et al.*, 1994; Resmini & Marsh, 1995; Higgins, 1996*a*, 1996*b*; Waters & Boudreau, 1996; Wilhelm & Wörner, 1996; Hammer *et al.*, 1999). Because different methods of CSD calculation were used in these studies, the numerical value of n° in different published sources cannot be compared directly. Therefore, the intercepts reported in the original publications have been replaced in Fig. 6 by normalized intercepts that also contain the constant C. The normalized intercept eliminates the effect of variable modal mineralogy and differing CSD measurement techniques. This effective intercept is equal to $\ln(n^\circ) + \ln(C)$, where $\ln(n^\circ)$ is the

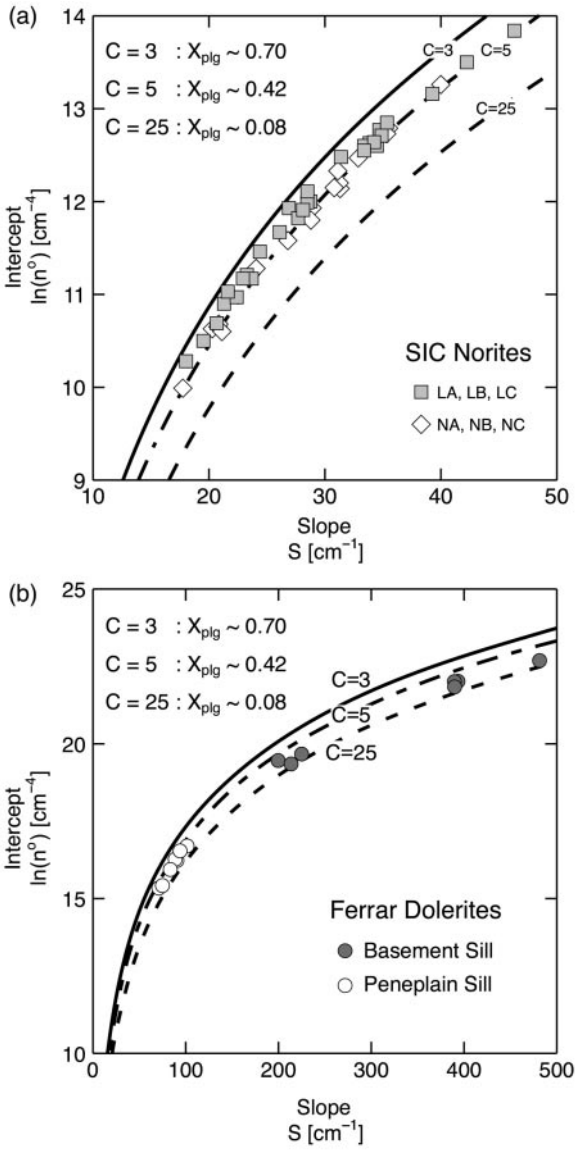

Fig. 5. Comparison of measured and predicted CSD intercepts and slopes. Measured values are from Table 1, predicted curves are from equation (19). (a) Sudbury Igneous Complex norite samples are fairly consistent at $C \approx 5$, corresponding to $X_{plg} \approx 0{\cdot}45$. (b) Ferrar Dolerite samples range from $C \approx 6{\cdot}5$ to 10, corresponding to $X_{plg} \approx 0{\cdot}35$–$0{\cdot}25$.

published CSD intercept and C is estimated from the entire published dataset using equation (13).

Although the agreement between the published CSDs and those measured in this study is not surprising in light of the fundamental nature of the scaling results, it does demonstrate the versatility of the method. All of the rocks measured for this study are intrusive, but the published data include both intrusive and extrusive rocks, with a range of composition from basaltic to dacitic. The volcanic rocks exhibit the same textural relationships as the plutonic rocks, without regard to composition, verifying that the textures of all rocks are governed by the same set of physical processes. Additionally, the various researchers each used a different routine for measuring and calculating CSDs. The variability in CSD technique has no effect on the validity of the relationships we have developed above. Finally, it should be noted that the chromite CSDs obey the same relationship as the plagioclase CSDs. The scaling relationships that have been developed are based on general kinetic and mass-balance considerations, and their usefulness is not limited to plagioclase in mafic intrusions.

DISCUSSION

A primary value of a scaling analysis is that it allows the behavior of complex systems to be studied even when the detailed mechanics are unknown. In the field of textural development, much progress has been made towards the goal of a complete predictive model of crystal nucleation and growth (e.g. Kirkpatrick, 1976; Dowty, 1980; Brandeis & Jaupart, 1987*a*, 1987*b*; Spohn *et al.*, 1988; Hort & Spohn, 1991; Hort, 1997; Toramaru, 2001). Despite these advances, there is not yet a general quantitative model capable of retrieving the cooling history of a magma from the texture of a rock. However, even without a detailed knowledge of the functional dependence of nucleation and growth rates on the thermal evolution of the magma, igneous textures can be quantitatively related to cooling history using the scaling relationships discussed above.

Prediction of texture variation

The most important variable controlling the development of igneous textures is time. More specifically, the characteristic size of crystals in a rock is controlled by the duration of the growth interval. Crystals will not nucleate at temperatures above the liquidus and are unlikely to grow appreciably below the solidus.

Given the relationship between CSD intercept and slope defined by equation (19) and depicted in Fig. 5, a full CSD can be calculated if either the slope or the intercept is known. The slope can be found from $\bar{L}$ using equation (12) and the mean length can be determined from a growth law and the crystallization interval Δt. This time Δt is therefore the fundamental constraint on the textural variation in an igneous body.

One common simplification used in cooling and solidification modeling is to reduce the problem to one-dimensional thermal diffusion in two adjacent semi-infinite regions. This corresponds to an infinite body of magma ($0 \leq z < \infty$) next to an infinite expanse of uniform country rock ($-\infty < z \leq 0$). This is a reasonable assumption when the distance from the margin is much

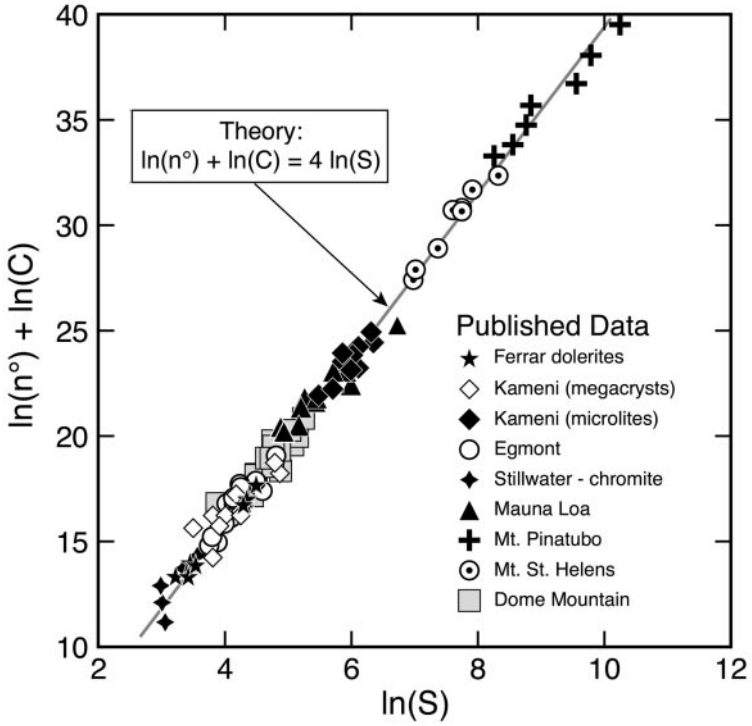

Fig. 6. CSD intercept–slope relationship from published data. CSDs from published studies follow the same trend as data measured in this study (Fig. 5). The effective intercept includes the constant C, which incorporates both modal and CSD calculation effects. Sources: Ferrar, Wilhelm & Wörner (1996); Kameni, Higgins (1996*b*); Egmont, Higgins (1996*a*); Stillwater, Waters & Boudreau (1996); Mauna Loa, Crisp *et al.* (1994); Mount Pinatubo, Hammer *et al.* (1999); Mount St. Helens, Cashman (1992); Dome Mountain, Resmini & Marsh (1995).

smaller than the thickness of the intrusion. In this case, the location of the liquidus and solidus isotherms as a function of time are described by an equation of the general form (Carslaw & Jaeger, 1959, p. 285)

$$z_\mathrm{i} = b_\mathrm{i}\sqrt{\kappa t} \tag{20}$$

where b_i is a constant that depends on the latent heat of crystallization and the initial temperatures of the magma and country rock. The subscript refers to the specific isotherm being considered. The functional form of the equation holds for any conductive cooling model, regardless of its level of sophistication.

The time at which the isotherms arrive at a point in space z can be obtained by rewriting equation (20):

$$t_\mathrm{i} = \frac{z^2}{\kappa b_\mathrm{i}^2}. \tag{21}$$

The time required for the temperature of the magma at position z to drop from the liquidus to the solidus is Δt:

$$\Delta t = t_\mathrm{s} - t_\mathrm{l} = \frac{z^2}{\kappa}\left(\frac{1}{b_\mathrm{s}^2} - \frac{1}{b_\mathrm{l}^2}\right) = \frac{z^2}{\kappa b^2} \tag{22}$$

which is the amount of time available for crystals to nucleate and grow at that location.

To replicate the variation in mean lengths that is observed in the Sudbury Igneous Complex, we use an expression that is slightly more complex than equation (5), but dimensionally identical:

$$\bar{L} = G^\circ(\Delta t + \tau). \tag{23}$$

This growth law accounts for the fact that the margins of igneous intrusions are almost never glassy, and often do not even have a hard chill. The presence of coarse-grained marginal rocks indicates that the solidus did not immediately propagate into a cooling intrusion, and therefore $\Delta t(z = 0) \neq 0$, which apparently contradicts equation (22).

Thermal models show that the contact of a cooling magma chamber remains at a constant temperature for a long period, usually until the center of the intrusion has begun to cool (Jaeger, 1968). The contact temperature is approximately the average of the initial temperatures of the magma and country rock. Therefore, if either the magma or the country rock starts at a sufficiently high temperature, it is possible for the contact temperature to start above the solidus of the magma, where it may then spend a significant length of time before cooling further. This effect is reflected in the parameter τ, which will be larger with higher initial temperatures (higher contact

Table 2: Physical parameters used in texture model

Parameter	Symbol	Value
Thermal diffusivity	κ	10^{-2} cm^2/s
Isotherm constant	b	0·475
Effective growth rate	G°	$1{\cdot}55 \times 10^{-14}$ cm/s
Time constant	τ	$1{\cdot}79 \times 10^{12}$ s

temperature) and with thicker intrusions (longer time until the contact begins to cool). The effect can also be related to observed physical properties of the system by noting that the product $G^\circ\tau$ is, in effect, the mean size of the crystals at the contact. If the magma does quench to a glass at the contact, then $\tau = 0$.

Any reasonable growth model could be substituted in place of equation (23). If desired, a detailed time-dependent growth model could be tested using measured CSD profiles. To evaluate this type of growth model, however, it would be necessary to have a nucleation model as well because the two processes operate together to produce the final texture. The interdependence of nucleation and growth rates and the use of these rate equations to predict a CSD were thoroughly discussed by Marsh (1998). In this study, however, the purpose is not to determine the details of crystallization history, but to provide a concise method for quantitatively relating the ultimate texture of a rock to the overall cooling history using a few simple parameters.

An example of the application of the scaling relationships and a growth law to the prediction of textural variations is shown in Fig. 7. We have used the simplified cooling model of equation (22) to calculate the variation in solidification time as a function of distance from the contact in the Sudbury Igneous Complex. Physical parameters for the model are listed in Table 2. The value of b was verified by comparison of the analytical solution with a full numerical cooling model (Zieg, 2001). The results of the cooling model were then used to obtain values for G° and τ by comparing measured textures of felsic norites to the calculated solidification times.

The variation in mean crystal size was then used to calculate the CSD slope and intercept using equations (12) and (19), together with the measured mineralogy of each rock. Because the slope and intercept fully describe the first-order characteristics of the CSD, the accuracy of the model can be tested by comparing the measured and predicted variations in slope and intercept as a function of distance from the contact. The calculated profiles in Fig. 7c and d match the measured data very well, indicating that the variation in texture within an intrusion can be predicted accurately using only a cooling model and a growth law. The irregularities in the calculated intercept profile are caused by the incorporation of measured plagioclase modes into the calculations (through C). These irregularities are of the same amplitude as irregularities in the measured intercepts, and demonstrate the sensitivity of this model. In this particular example, the growth law was constrained by measured data, but the method could just as easily be used to predict textural variations with an independent estimate of G° and τ.

Within an intrusion, the slope and intercept vary systematically with distance from the margin. They are highest near the contact, where the cooling was rapid, and lowest in the interior of the body, where cooling was slow. This suggests that the CSDs of a sample can be used to determine the solidification time Δt. The solidification time can then be related to the position of a sample with respect to the margin. Therefore, a series of textures can be used to determine the relative positions of the samples.

Interpretation of volcanic textures

In contrast to plutonic rocks, volcanic rocks generally cannot be uniquely associated with a specific position in a magma chamber. However, because the crystallization process is the same in both systems, the texture of a volcanic rock also records the thermal history of the sample. The challenge is to use a series of distinct lava flows to obtain information about the spatial and temporal variations in a subvolcanic magma chamber.

As discussed previously, differences in cooling regime reflect differences in position, and lead to differences in texture. When a set of textures obeying the general intercept–slope relationship are plotted simultaneously on a CSD, they appear to fan (Fig. 8). The position of the individual CSD within the fan is related to its position within the intrusion, and therefore to the cooling history of the sample.

It is not uncommon to find fanning CSDs in suites of comagmatic volcanic rocks (Marsh *et al.*, 1995). Two examples are suites from the Atka volcanic center in the Aleutians (Myers *et al.*, 1986; Marsh, 1998) and from Ocean Drilling Program (ODP) Hole 504B in the Costa Rica rift (Marsh & Liu, 1999). Both suites show CSDs that closely resemble the calculated fan and the SIC fan (Fig. 9). Although the volcanic CSDs from Atka and Hole 504B show the same pattern as the intrusive CSDs from Sudbury, the interpretation is not as straightforward. Specifically, it is difficult to separate the effects of varying residence times and varying positions within the chamber.

To use volcanic CSDs as meaningful indicators of magma chamber processes, it is important to distinguish

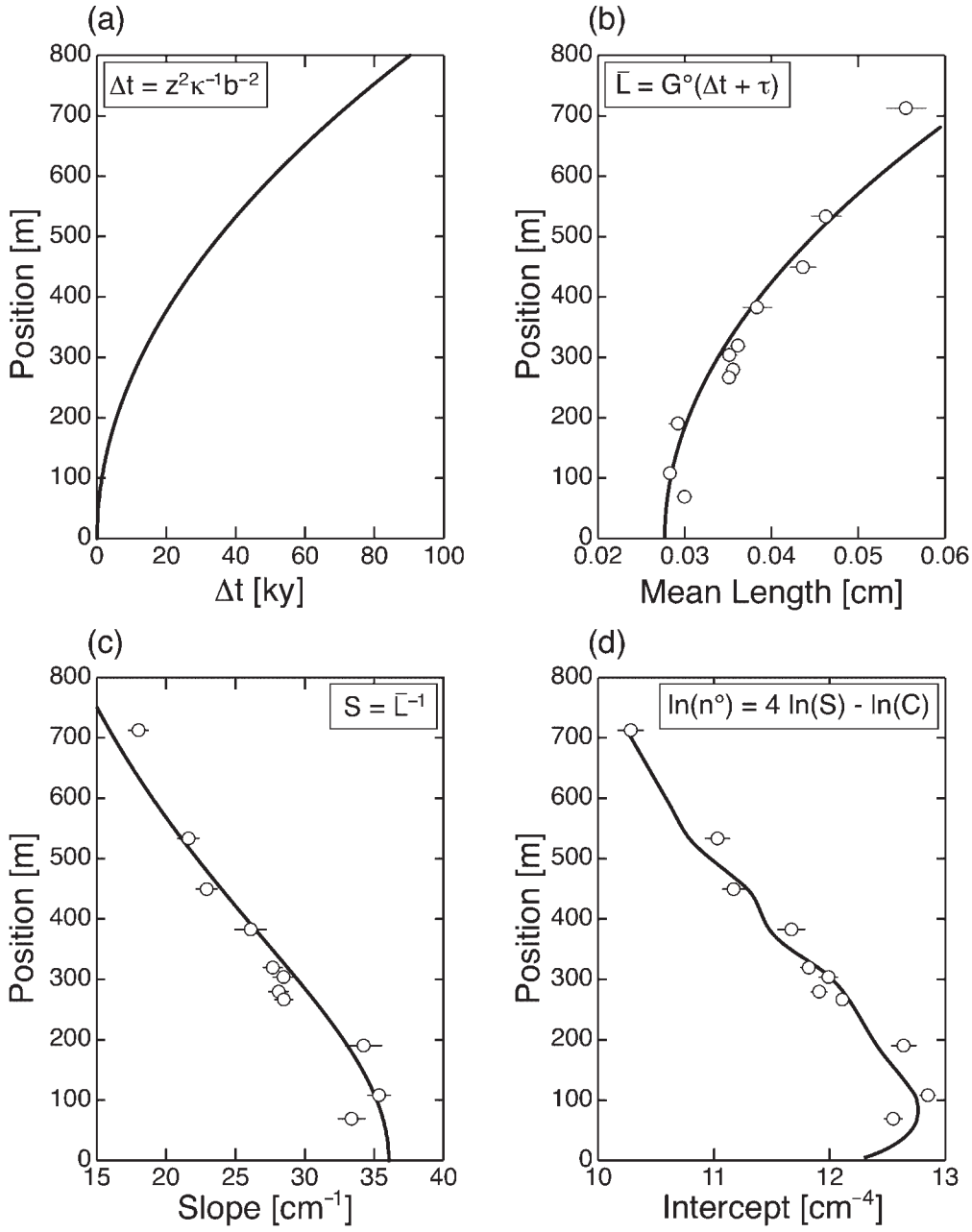

Fig. 7. Model and measured textural profiles. The continuous lines represent model predictions and the symbols indicate measured data. The data are obtained from drill core LA in the Sudbury Igneous Complex. (a) The solidification interval Δt is calculated as a function of distance from the contact using equation (22) and the parameters in Table 2. (b) The mean length is calculated from the solidification interval using equation (23). G° and τ are obtained from measured data. (c) CSD slope is related to mean length of the crystals through equation (12). (d) CSD intercept can be predicted from the slope using equation (19). In this example, the model curve has been modified by incorporating the measured plagioclase abundances.

between samples taken from the same location at different system ages, and samples taken from different locations at roughly the same time. The modal plagioclase (X_{plg}) plays a vital role in making this distinction because crystallinity increases with time at a fixed point in space and with proximity to the margin at a fixed time. The interaction between intercept, slope, and crystallinity will reflect the cooling regime (i.e. cooling rate and system age) at the position within the magma chamber from which the lava was erupted. A full treatment of this

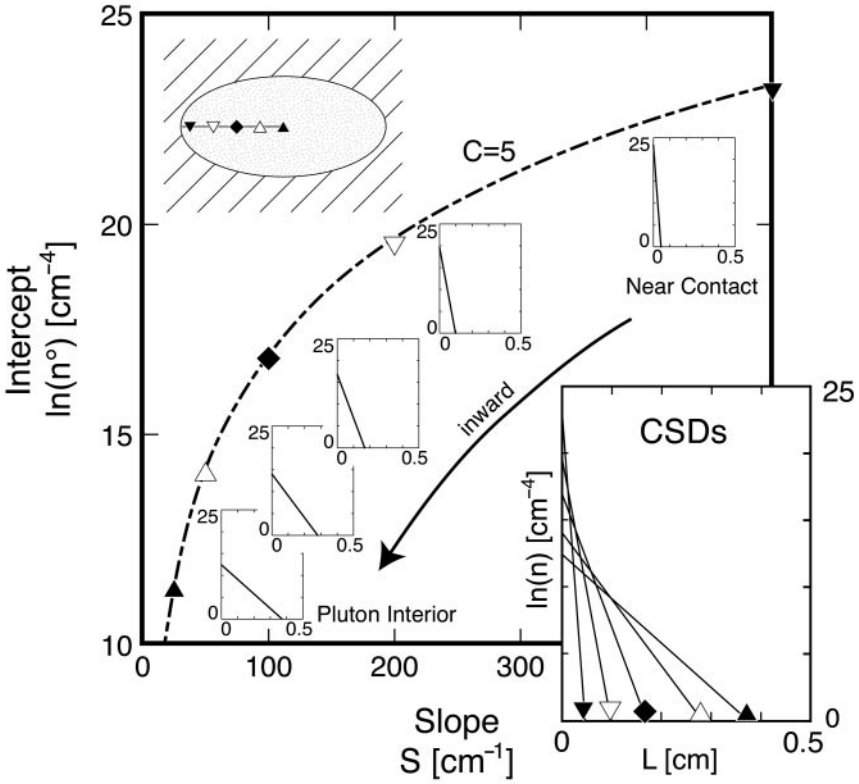

Fig. 8. Application of intercept–slope equation. Each point along the curve represents an idealized CSD. Moving along the curve corresponds to changing spatial position within the intrusion, or to changing the cooling history of the magma. When a series of predicted CSDs is plotted together, it results in a fanning pattern. The position within the fan corresponds to a particular thermal regime, or equivalently, a particular position within the intrusion. The relationship can be quantified by relating the slope to the cooling interval through a growth model.

problem is beyond the scope of this paper, but it demonstrates a potential application of the methods outlined above.

Characteristic nucleation and growth rates

Cashman (1993) has discussed the dependence of plagioclase growth and nucleation rates on the local cooling rate. The kinetic parameters were obtained from the textures of the rocks and the cooling rates are calculated as kz^{-2}, with a value for k between 0·135 and 0·822. In other words, the cooling rate $(\partial T/\partial t)$ is inversely proportional to the cooling duration Δt. The total temperature interval of crystallization (ΔT) is constant; the only variable is the length of time required for the temperature change (Δt). The growth and nucleation rates were determined by dividing the characteristic lengths and numbers by the cooling duration.

The data from Table 1 can be used to calculate growth and nucleation rates using a similar procedure. Using the relationships developed above, we obtain the following equations for $\mathcal{J}_0$ and G_0 in terms of the slope and intercept of the CSD and the solidification interval Δt:

$$\mathcal{J}_0 = \frac{c_1 N_0}{t_c} = \frac{c_1\, n^\circ}{S\Delta t} \tag{24}$$

$$G_0 = \frac{c_2\, L_0}{t_c} = \frac{c_2}{S\Delta t}. \tag{25}$$

Equation (22) expresses Δt in terms of position within the intrusion, which allows equations (24) and (25) to be rewritten in terms of z:

$$\mathcal{J}_0 = \frac{c_1 \kappa n^\circ}{S z^2} \tag{26}$$

$$G_0 = \frac{c_2 \kappa}{S z^2}. \tag{27}$$

These groups, which represent characteristic rates, could be used to form dimensionless nucleation and growth rates in other problems. We now define two new variables, $\mathcal{J}^*$ and G^*, which are not strictly rate parameters, but are related to the rates of nucleation and growth through the thermal diffusivity κ and the dimensionless constants c_1 and c_2 (into which b has been incorporated):

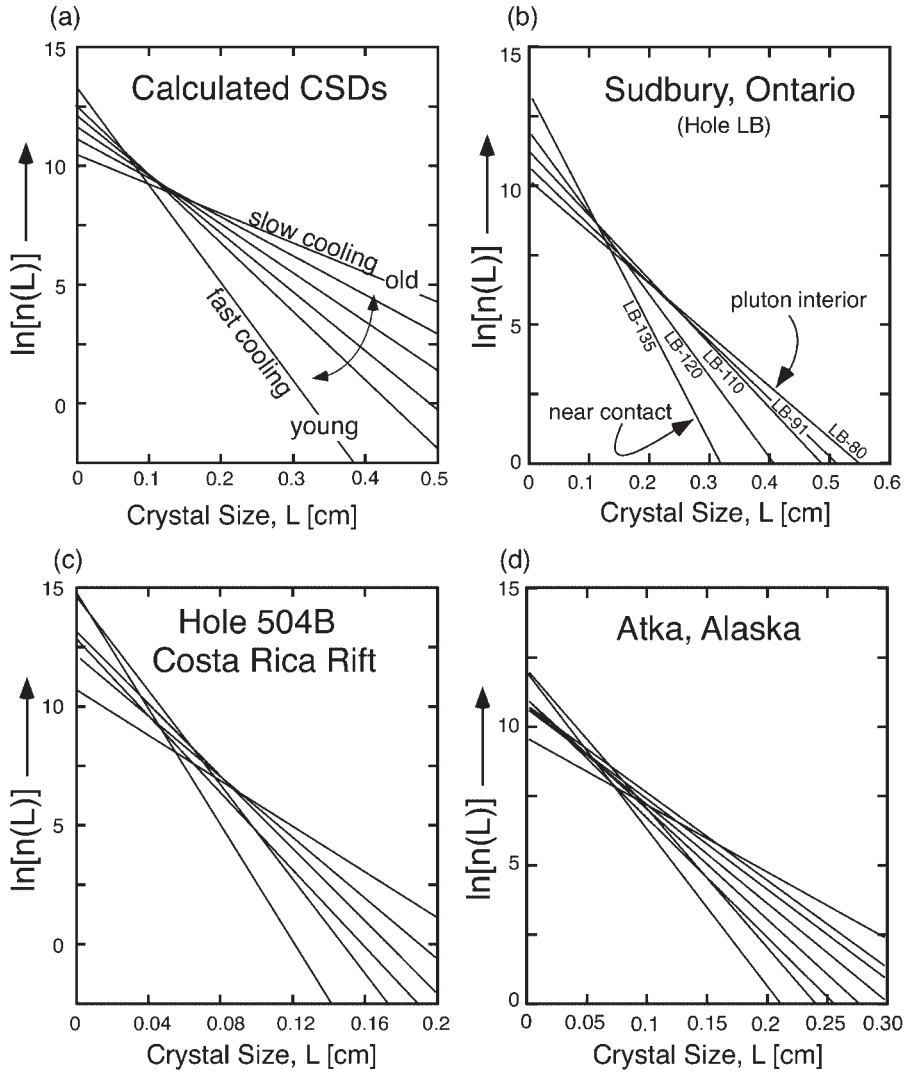

Fig. 9. Fanning CSDs. (a) Calculated CSD fan, with each CSD represented by a straight line corresponding to a single point along the intercept–slope curve (e.g. Fig. 8). The different CSDs correspond to different cooling regimes. (b) CSDs of plutonic rocks of the Sudbury Igneous Complex show a pattern similar to the calculated fan. In this case, the position in the fan can be correlated directly with the position within the intrusion. (c, d) CSDs of volcanic rocks from the Costa Rica rift and the Atka volcanic center, Alaska. Although the same fanning pattern is observed as in the plutonic rocks, the position in the fan cannot necessarily be directly related to the position in the magma chamber from which the lava was derived without considering the degree of crystallization.

$$\mathcal{J}^* = \frac{\mathcal{J}_0}{c_1\kappa} = \frac{n^\circ}{Sz^2} \tag{28}$$

$$G^* = \frac{G_0}{c_2\kappa} = \frac{1}{Sz^2}. \tag{29}$$

The new nucleation parameter $\mathcal{J}^*$ has units of cm^{-5} and the new growth parameter G^* has units of cm^{-1}. Figure 10 shows $(\mathcal{J}^*)^{-1/5}$ and $(G^*)^{-1}$ plotted as a function of distance from the margin for samples from Sudbury drill hole LA and the Peneplain Sill transect from Antarctica. The linearity of the relationship between $(\mathcal{J}^*)^{-1/5}$ and z in Fig. 10a indicates that the nucleation rate is correctly scaled in the equations above. It is still unclear whether the deviation from linearity in Fig. 10b is significant. If significant, it may indicate that equations (5) and (23) are not entirely correct, in which case the mean length of crystals in a rock may be related to time in a nonlinear fashion. In fact, there is no reason to assume that this would not be the case. But, regardless of how Fig. 10b is interpreted, the basic assumption ($L \propto \Delta t$) of the model is sufficient to accurately predict most of the textural variation in the two intrusions.

A final observation is that the variation in G^* is on the order of 50, and the variation in $\mathcal{J}^*$ is on the order of 500. Given the difficulty of measuring growth

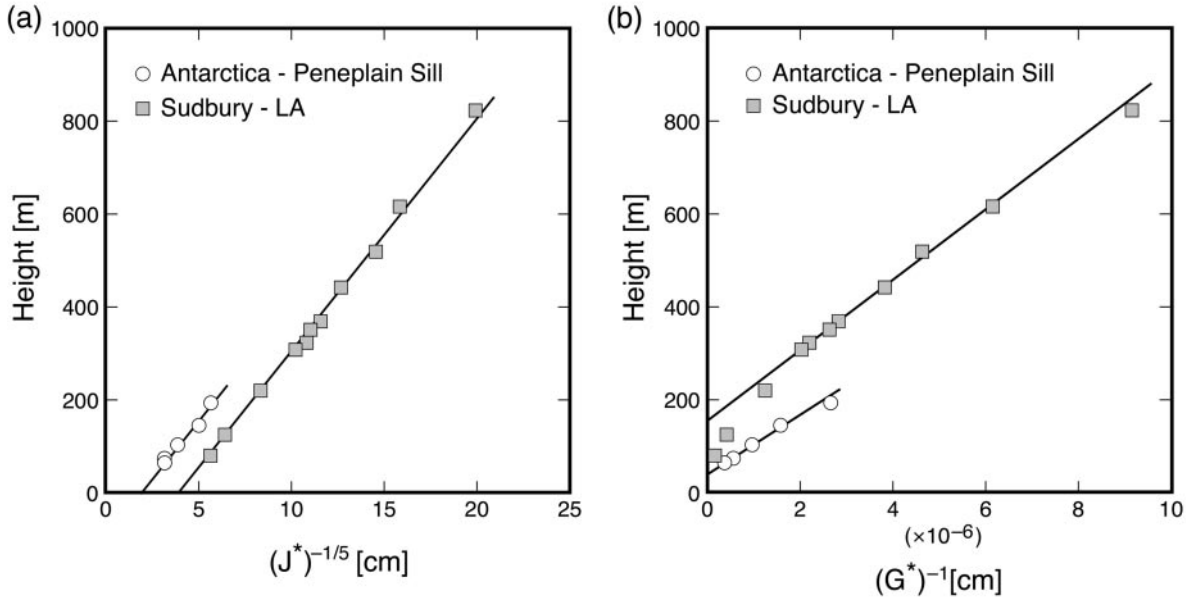

Fig. 10. Kinetic data as derived from CSDs and sample position. (a) Nucleation parameter, $(J^*)^{-1/5}$, as a function of position. The same trend in nucleation rates is apparent for rocks from the Ferrar Dolerite (Peneplain Sill) and the Sudbury Igneous Complex (drill core LA). Nucleation rate is greatest near the contact and decreases with distance from the margin. (b) Growth parameter, $(G^*)^{-1}$, as a function of distance from the margin. The trend is linear in the Antarctic samples, but not in the Sudbury samples. The departure from linearity indicates that equation (23) may not always hold precisely. However, the total range in G^* is extremely narrow.

or nucleation rates, this range of values is small enough to treat these parameters as constants for the purpose of scaling. Therefore, the assumptions made in equations (1) and (2) can be justified. Although the characteristic nucleation and growth rates are not constant throughout an intrusion, over a nearly 1 km section of norite in the Sudbury Igneous Complex, the maximum variation is less than three orders of magnitude. As seen in Fig. 7, even if the effective growth rate is taken to be a universal (instead of local) constant, the measured variation in textures can be predicted with a high degree of accuracy.

CONCLUSIONS

Scaling or dimensional analysis (e.g. Barenblatt, 1996) allows fundamental relationships to be found between key parameters in kinetic systems without a detailed formulation of the actual processes of crystal nucleation and growth. Although many of the relationships shown here were previously known, the consistent incorporation of quantitative measures of total crystal numbers (N_T) and mean crystal size ($\bar{L}$) allows the relationship between them to be calibrated using information from plagioclase in mafic rocks. This scaling also allows a unique relation to be defined between CSD slope and intercept, the existence of which has long been suspected from CSD observations (e.g. Marsh, 1998; Higgins, 1999). Because CSD slope is directly linked to $\bar{L}$ and slope is related to the intercept, a full CSD for plutonic rocks can be found by incorporating a crystal growth law into any model of solidification.

In fact, the dependence of CSDs on $\bar{L}$ is the key to relating textures to the cooling process. Specifically, it means that any model that predicts $\bar{L}$ as a function of position in a pluton or as a function of time for a volcanic sequence can be used to generate a hypothetical series of textures. Deviations between predicted and measured textures reveal additional processes beyond simple nucleation and growth that have contributed to the final CSD. These processes may include, for example, crystal sorting or resorption of small crystals. The spatial variation of textures within a sill or pluton may also reveal multiple cooling or injection events. Because the prevailing local thermal regime, or solidification time, is the key factor controlling $\bar{L}$, a suite of CSDs will exhibit a systematic fanning pattern within any magmatic body. This characteristic feature, which is common in comagmatic volcanic suites, may allow the relative spatial positions of the volcanic rocks to be estimated in the preeruptive parent body. It could also allow an estimate of the local cooling rate in the parent magma, which would be particularly useful to know along the ocean ridges.

The fundamental value of these results is that, despite a lack of the complete information needed for a quantitative kinetic model of crystallizing magmatic systems, a critical

quantitative link has been made between rock texture, cooling history, and phase equilibria.

ACKNOWLEDGEMENTS

The authors would like to acknowledge the constructive comments and suggestions of J. E. Hammer, Y. Liang, M. D. Higgins, and D. A. Jerram. We are indebted to Falconbridge, Inc. for their extensive generosity in sharing these and many other samples from the Sudbury Igneous Complex, as well as for their greatly appreciated funding support. This work was supported by grants from the National Science Foundation (EAR-9725158, OPP-9814332, OCE-9711575) to B.D.M.

REFERENCES

Ariskin, A. A., Frenkel, M. Y., Barmina, G. S. & Nielsen, R. L. (1993). COMAGMAT; a Fortran program to model magma differentiation processes. *Computers and Geosciences* **19**, 1155–1170.

Barenblatt, G. I. (1996). *Scaling, Self-similarity, and Intermediate Asymptotics*. New York: Cambridge University Press.

Bowen, N. L. (1922). The reaction principle in petrogenesis. *Journal of Geology* **30**, 177–198.

Brandeis, G. & Jaupart, C. (1987*a*). Crystal sizes in intrusions of different dimensions: constraints on the cooling regime and the crystallization kinetics. In: Mysen, B. O. (ed.) *Magmatic Processes: Physicochemical Principles*. University Park, PA: Geochemical Society, pp. 307–318.

Brandeis, G. & Jaupart, C. (1987*b*). The kinetics of nucleation and crystal growth and scaling laws for magmatic crystallization. *Contributions to Mineralogy and Petrology* **96**, 24–34.

Carslaw, H. S. & Jaeger, J. C. (1959). *Conduction of Heat in Solids*, 2nd edn. New York: Oxford University Press.

Cashman, K. V. (1992). Groundmass crystallization of Mount St. Helens dacite 1980–1986: a tool for interpreting shallow magmatic processes. *Contributions to Mineralogy and Petrology* **109**, 431–449.

Cashman, K. V. (1993). Relationship between plagioclase crystallization and cooling rate in basaltic melts. *Contributions to Mineralogy and Petrology* **113**, 126–142.

Crisp, J., Cashman, K. V., Bonini, J. A., Hougen, S. B. & Pieri, D. C. (1994). Crystallization history of the 1984 Mauna Loa lava flow. *Journal of Geophysical Research* **99**, 7177–7198.

Cross, W., Iddings, J. P., Pirsson, L. V. & Washington, H. S. (1903). *Quantitative Classification of Igneous Rocks*. Chicago, IL: University of Chicago Press.

Dietz, R. S. (1964). Sudbury Structure as an astrobleme. *Journal of Geology* **72**, 412–434.

Dowty, E. (1980). Crystal growth and nucleation theory and the numerical simulation of igneous crystallization. In: Hargraves, R. B. (ed.) *The Physics of Magmatic Processes*. Princeton, NJ: Princeton University Press, pp. 419–485.

Dressler, B. O., Weiser, T. & Brockmeyer, P. (1996). Recrystallized impact glasses of the Onaping Formation and the Sudbury Igneous Complex, Sudbury Structure, Ontario, Canada. *Geochimica et Cosmochimica Acta* **60**, 2019–2036.

Ghiorso, M. S. & Sack, R. O. (1995). Chemical mass transfer in magmatic processes. IV. A revised and internally consistent thermodynamic model for the interpolation and extrapolation of liquid–solid equilibria in magmatic systems at elevated temperatures and pressures. *Contributions to Mineralogy and Petrology* **119**, 197–212.

Gray, N. H. (1970). Crystal growth and nucleation in two large diabase dikes. *Canadian Journal of Earth Sciences* **7**, 366–375.

Gray, N. H. (1978). Crystal growth and nucleation in flash-injected diabase dikes. *Canadian Journal of Earth Sciences* **15**, 1904–1923.

Grieve, R. A. F. (1994). An impact model of the Sudbury Structure. In: Lightfoot, P. C. & Naldrett, A. J. (eds.) *Proceedings of the Sudbury–Noril'sk Symposium. Ontario Ministry of Northern Development and Mines Special Volume* **5**, 119–132.

Gunn, B. M. (1966). Modal and element variation in Antarctic tholeiites. *Geochimica et Cosmochimica Acta* **30**, 881–920.

Hammer, J. E., Cashman, K. V., Hoblitt, R. P. & Newman, S. (1999). Degassing and microlite crystallization during pre-climactic events of the 1991 eruption of Mt. Pinatubo, Philippines. *Bulletin of Volcanology* **60**, 355–380.

Higgins, M. D. (1996*a*). Crystal size distributions and other quantitative textural measurements in lavas and tuff from Egmont volcano (Mt. Taranaki), New Zealand. *Bulletin of Volcanology* **58**, 194–204.

Higgins, M. D. (1996*b*). Magma dynamics beneath Kameni volcano, Thera, Greece, as revealed by crystal size and shape measurements. *Journal of Volcanology and Geothermal Research* **70**, 37–48.

Higgins, M. D. (1999). Origin of megacrysts in granitoids by textural coarsening: a crystal size distribution (CSD) study of microcline in the Cathedral Peak granodiorite, Sierra Nevada, California. In: Fernandez, C. & Castro, A. (eds) *Understanding Granites: Integrating Modern and Classical Techniques. Geological Society, London, Special Publications* **168**, 207–219.

Higgins, M. D. (2000). Measurement of crystal size distributions. *American Mineralogist* **85**, 1105–1116.

Hort, M. (1997). Cooling and crystallization in sheet-like magma bodies revisited. *Journal of Volcanology and Geothermal Research* **76**, 297–317.

Hort, M. & Spohn, T. (1991). Crystallization calculations for a binary melt cooling at constant rates of heat removal: implications for the crystallization of magma bodies. *Earth and Planetary Science Letters* **107**, 463–474.

Jaeger, J. C. (1968). Cooling and solidification of igneous rocks. In: Hess, H. H. & Poldervaart, A. (eds) *Basalts: the Poldervaart Treatise on Rocks of Basaltic Composition*. New York: Interscience, pp. 503–536.

Kirkpatrick, R. J. (1976). Towards a kinetic model for magma crystallization. *Journal of Geophysical Research* **81**, 2565–2571.

Kirkpatrick, R. J. (1983). Kinetics of crystallization of igneous rocks. In: Lasaga, A. C. & Kirkpatrick, R. J. (eds) *Kinetics of Geochemical Processes*. Washington, DC: Mineralogical Society of America, pp. 321–398.

Lane, A. C. (1899). The grain of rocks. *Michigan Geological Survey, Geological Report on Isle Royale* **6**, 106–121.

Lane, A. C. (1903). Studies of the grain of igneous intrusives. *Geological Society of America Bulletin* **14**, 369–384.

Lane, A. C. (1928). Genetic significance of grain. *Tufts College Studies* **5**, 112–131.

Marsh, B. D. (1988). Crystal size distribution (CSD) in rocks and the kinetics and dynamics of crystallization I. Theory. *Contributions to Mineralogy and Petrology* **99**, 277–291.

Marsh, B. D. (1998). On the interpretation of crystal size distributions in magmatic systems. *Journal of Petrology* **39**, 553–599.

Marsh, B. D. (2000). Magma chambers. In: Sigurdsson, H., Houghton, B., McNutt, S. R., Rymer, H. & Stix, J. (eds.) *Encyclopedia of Volcanoes*. San Diego, CA: Academic Press, pp. 191–206.

Marsh, B. D. & Liu, L. (1999). Ridge magmatism: Atlantic vs. Pacific as recorded by crystal size distributions (CSDs). *EOS Transactions, American Geophysical Union* **80**, S344.

Marsh, B. D. & Philipp, J. R. (1996). Three-dimensional magmatic filling of Basement sill revealed by unusual crystal concentrations. *Antarctic Journal* **31**, 39–41.

Marsh, B. D., McCormick, K. A. & Resmini, R. (1995). Pivot points in crystal size distributions and solidification fronts and texture development in igneous rocks. *EOS Transactions, American Geophysical Union* **76**, S293.

Myers, J. D., Marsh, B. D. & Sinha, A. K. (1986). Geochemical and strontium isotopic characteristics of parental Aleutian Arc magmas: evidence from the basaltic lavas of Atka. *Contributions to Mineralogy and Petrology* **94**, 1–11.

Naldrett, A. J. & Kullerud, G. (1967). A study of the Strathcona mine and its bearing on the origin of the nickel–copper ores of the Sudbury District, Ontario. *Journal of Petrology* **8**, 456–531.

Naldrett, A. J., Bray, J. G., Gasparrini, E. L., Podolsky, T. & Rucklidge, J. C. (1970). Cryptic variation and the petrology of the Sudbury Nickel Irruptive. *Economic Geology* **65**, 122–155.

Pye, E. G., Naldrett, A. J. & Giblin, P. E. (eds) (1984). *The Geology and Ore Deposits of the Sudbury Structure. Ontario Geological Survey, Special Volume* **1**.

Queneau, A. L. (1902). Size of grain in igneous rocks in relation to the distance from the cooling wall. *Columbia University School of Mines Quarterly* **23**, 181–195.

Randolph, A. D. & Larson, M. A. (1988). *Theory of Particulate Processes*, 2nd edn. New York: Academic Press.

Resmini, R. G. & Marsh, B. D. (1995). Steady-state volcanism, paleo-effusion rates, and magma system volume inferred from plagioclase crystal size distributions in mafic lavas: Dome Mountain, Nevada. *Journal of Volcanology and Geothermal Research* **68**, 273–296.

Spohn, T., Hort, M. & Fischer, H. (1988). Numerical simulation of the crystallization of multicomponent melts in thin dikes or sills 1. The liquidus phase. *Journal of Geophysical Research* **93**, 4880–4894.

Swanson, S. E. (1977). Relation of nucleation and crystal-growth rate to the development of granitic textures. *American Mineralogist* **62**, 966–978.

Toramaru, A. (2001). A numerical experiment of crystallization for a binary eutectic system with application to igneous textures. *Journal of Geophysical Research* **106**, 4037–4060.

Waters, C. & Boudreau, A. E. (1996). A reevaluation of crystal size distributions in chromite cumulates. *American Mineralogist* **81**, 1452–1459.

Wilhelm, S. & Wörner, G. (1996). Crystal size distribution in Jurassic Ferrar flows and sills (Victoria Land, Antarctica): evidence for processes of cooling, nucleation, and crystallisation. *Contributions to Mineralogy and Petrology* **125**, 1–15.

Winkler, H. G. F. (1949). Crystallization of basaltic magma as recorded by variation of crystal sizes in dikes. *Mineralogical Magazine* **28**, 557–574.

Zieg, M. J. (2001). Cooling and crystallization of the Sudbury Igneous Complex. Ph.D. dissertation, Johns Hopkins University, Baltimore, MD.